

Quantifying Choriocapillaris Flow Deficits in Diabetic Retinopathy Using Projection-Resolved OCT Angiography

Jie Wang,¹ Tristan Hormel,¹ Dong-Wouk Park,¹ Shazib Haq,¹ Steve Bailey,¹ David Huang,^{1,2} Thomas S. Hwang,¹ and Yali Jia^{1,2}

¹Casey Eye Institute, Oregon Health & Science University, Portland, Oregon, United States

²Department of Biomedical Engineering, Oregon Health & Science University, Portland, Oregon, United States

Correspondence: Yali Jia, Casey Eye Institute, Oregon Health & Science University, 515 SW Campus Dr., Portland, OR 97239, USA;
jiaya@ohsu.edu.

JW and TH share first authorship.

Received: October 6, 2024

Accepted: August 2, 2025

Published: September 4, 2025

Citation: Wang J, Hormel T, Park DW, et al. Quantifying choriocapillaris flow deficits in diabetic retinopathy using projection-resolved OCT angiography. *Invest Ophthalmol Vis Sci.* 2025;66(12):13.

<https://doi.org/10.1167/iovs.66.12.13>

PURPOSE. To quantify choriocapillaris (CC) flow deficits using projection-resolved optical coherence tomographic angiography (PR-OCTA) and to evaluate whether they are correlated with diabetic retinopathy (DR).

METHODS. In this retrospective study, OCTA scans covering a range of DR severities were acquired. Shadowing artifacts caused by hard exudates, large inner retinal vessels, and vitreous floaters were detected, along with the retinal fluid area. The CC deficit ratio (percentage of deficit area) was measured and compared with shadowing artifacts and area beneath retinal fluid excluded to assess the effect of these confounding features. The Spearman correlation between the CC deficit ratio and disease severity was calculated, as well as the diagnostic performance (area under the receiver operating characteristic curve).

RESULTS. One hundred eighty-three participants were enrolled in this study. We found a significant positive correlation between age and CC deficit ratio in normal controls (Pearson correlation, $P = 0.02$). There was no significant difference in deficit ratio between measurements excluding only shadows and those excluding both shadows and the area beneath the fluid (Mann-Whitney U-test, $P = 0.81$). The CC deficit ratio was positively correlated with DR severity (Spearman correlation, $P < 0.01$). It was significantly higher in nonproliferative DR and PDR patients compared to normal controls (Tukey HSD, $P < 0.01$) but not in those with diabetes without DR. The proposed CC deficit segmentation method achieved high repeatability with an intraclass correlation coefficient of 0.92.

CONCLUSIONS. The CC deficit ratio measured by the proposed method correlates with the presence and severity of DR.

Keywords: choriocapillaris flow deficits, projection-resolved OCT angiography, diabetic retinopathy

Diabetic retinopathy (DR) is the most common complication of diabetes mellitus and is the leading cause of vision loss in working-age individuals.¹ In most cases, this vision loss can be prevented with timely intervention.² With the number of people living with DR expected to reach 160 million globally in the coming decades,³ effective screening and improvement in the management of DR are critical in reducing the burden of this disease.

Optical coherence tomography (OCT) and OCT angiography (OCTA), which can both be obtained simultaneously from the same scan, are widely adopted in the diagnosis and management of DR. OCT is a noninvasive and inexpensive⁴ imaging modality that provides high-resolution and depth-resolved images of the retina. Because OCTA is a functional extension based on repeated OCT scans, it inherits all these advantages but comes with the additional ability to sharply delineate vasculature. Both OCT and OCTA have demonstrated benefits for the diagnosis and management of DR. Structural OCT is essential for identifying diabetic macular edema (DME) and assessing response

to treatment.⁵ OCTA can accurately delineate neovascularization without losing information due to leakage seen in dye-based angiography.^{6,7} In addition to neovascularization and macular edema, which are most strongly associated with vision loss in DR, OCTA can visualize other key pathologic features, such as non-perfusion areas,^{8,9} intraretinal microvascular abnormalities,¹⁰ and microaneurysms.^{11–13} These clinical abnormalities can be useful for staging the disease and could provide the foundation for personalized interventions.¹⁴

Although the majority of the clinical research on DR has focused on retinal pathologies, we know from histologic studies that diabetes affects the choroid.¹⁵ The choriocapillaris endothelium is a major source of vascular endothelial growth factor in DR, which may contribute to both neovascularization and macular edema.¹⁶ In addition, loss of choriocapillaris has been reported in DR.¹⁷ Structural OCT has also been used to analyze choroidal changes in DR and is notably capable of correlating choroidal thinning with advanced disease states.^{18,19} Dye-based angiography, such as



indocyanine green angiography, has limited ability to investigate the choroidal vasculature, particularly the choriocapillaris, due to its limited axial imaging resolution in microvascular networks and blockage caused by leakage from the overlying retinal capillary plexuses.^{20,21} OCTA, however, is uniquely suited for visualizing the choriocapillaris (CC) in vivo.²²

OCTA measurements in the CC face substantial challenges that must be addressed. First, the extreme density of CC (it transports the most blood per unit weight of any tissue in the body²³) makes the resolution of individual vessels impossible, meaning metrics used in the retinal vasculature, such as nonperfusion area or vessel tortuosity, cannot be obtained. An alternative method to detect the localized decrease in flow, such as flow deficit, must be used.^{24–26} The CC is located immediately posterior to retinal pigment epithelium (RPE) and Bruch's membrane (BM), the highly reflective tissue that both attenuates flow signal and produces strong projection artifacts.²⁷ Because flow deficits are identified by detecting pixels that lack flow signals, local flow signal loss due to shadowing must also be considered.²⁸ Here, we present a new flow deficit segmentation technique that accounts for both projection and shadow artifacts and examines the resulting measurements against DR severity and DME.

METHODS

Recruitment Criteria and Data Acquisition

Patients with DR were recruited with informed consent from the Casey Eye Institute, Oregon Health and Science University, Portland, OR, USA. Participants underwent clinical examinations and combined OCT/OCTA imaging using a commercial device (Solix; Visionix USA, Lombard, IL, USA), a spectral domain system with 840-nm central wavelength and a 120-kHz A-line scanning rate. Macular scans, centered on the foveal avascular zone, covered a 6.4×6.4 -mm area and were captured with 512×512 -pixel resolution. Two consecutive B-scans were obtained at the same location, and the commercial split-spectrum amplitude-decorrelation angiography algorithm was applied to calculate the flow signal by analyzing variations between them.²⁹ Additionally, one X-Fast and one Y-Fast volume were acquired, registered, and merged to remove motion artifacts.³⁰ Auto-focusing was enabled during imaging acquisition, and en face OCTA images were reviewed to confirm adequate focus. Normal controls were determined with retinal specialists in the Casey Eye Institute clinic. DR severity was determined by a retinal specialist (author TSH) and divided into five categories based on ETDRS criteria: normal controls, diabetes without retinopathy, nonproliferative DR (NPDR), and proliferative DR (PDR). The eyes with DME were also detected based on the DR standards for central macular thickness. This study was approved by an institutional review board and complied with the Declaration of Helsinki.

Retina Layers Segmentation and Artifact Removal

Retinal layer segmentation, projection artifact removal, and shadowing artifact detection are essential pre-processing steps for accurately quantifying CC deficits, as each can lead to quantification errors. Incorrect retinal layer segmentation can map the wrong anatomic regions to an en face image,

which is detrimental to any quantification targeting a specific tissue like the CC. In this work, retinal layers, including the inner limiting membrane, inner plexiform layer/outer plexiform layer (OPL), OPL/outer nuclear layer (ONL), and BM were segmented using an automated graph search-based algorithm for generating en face OCT and OCTA images.³¹ The segmentation errors were then manually corrected by author JW using the intelligent manual correction function that is implemented in our in-house Center for Ophthalmic Optics & Lasers OCTA Reading Toolkit (COOL-ART) software. The retinal layers segmented here, while not directly related to producing en face CC images, are useful for our shadow and projection artifact compensation strategies, which rely on additional images. Two types of en face OCTA were generated: (1) a superficial vascular complex (SVC) angiogram comprising the anterior 80% of the ganglion cell complex (combined GCL and inner plexiform layer) anatomic slab, and (2) the CC, comprising the slab between the BM and BM + 10 μm . Two types of en face OCT were generated: (1) the slab containing deep capillary plexus (DCP), defined within the outer 50% of the INL and the entire OPL, and (2) an RPE slab, defined within the BM-25 μm and BM. En face OCT was generated by mean projection, whereas en face OCTA was generated by maximum projection.³²

Projection artifacts are a major concern for flow deficit detection since they can lead to false negative flow deficit detections when superficial vasculature introduces a spurious flow signal in a region that lacks in situ flow. Projection artifacts were cleaned using the projection-resolved OCTA (PR-OCTA) algorithm.³³ This algorithm models the flow signal as a combination of in situ and artifactual flow, enabling volumetric estimation and subsequent removal of artifactual components. The resultant en face images retain high vessel connectivity, indicating the minimal loss of in situ flow signal caused by over-processing. Moreover, images of the separate anatomic vascular layers, such as the SVC, intermediate capillary plexus, DCP, and CC, each with different vascular patterns, demonstrate low flow signal correlation. This indicates the effective removal of duplicated vascular patterns.³³

Shadow artifacts can yield false-positive flow deficit detections because of artifactual signal loss. The in situ flow is not recoverable because the signal is lost in shadowed regions. The best option is to exclude such regions from the analysis because they could introduce artificial flow deficits. Shadow artifacts can result from several pathologies related to DR or from unrelated pathologies that may occur simultaneously, including hard exudates, floaters, or microaneurysms. Even in regions without pathology, shadows can form under large vessels. In this work, shadow artifacts were identified using a method that combines structural and angiographic en face image inputs (Fig. 1). Hard exudates, appearing as hyperreflective objects in the DCP slab, cause shadows in the RPE and CC images. To mitigate the brightness variation caused by differences in signal strength variation, en face OCT images were normalized using a dynamic display range defined as the [0.5th percentile, 99.5th percentile], while en face OCTA images were normalized using a range defined as the [2.5th percentile, 97.5th percentile]. Hyperreflective objects were enhanced by multiplying the en face structural images with the reflectance-reversed en face RPE image, and detected using blob-like feature detection.³⁴ Vitreous floaters, which cast shadows in the RPE slab, also appear as hyperreflective objects in the

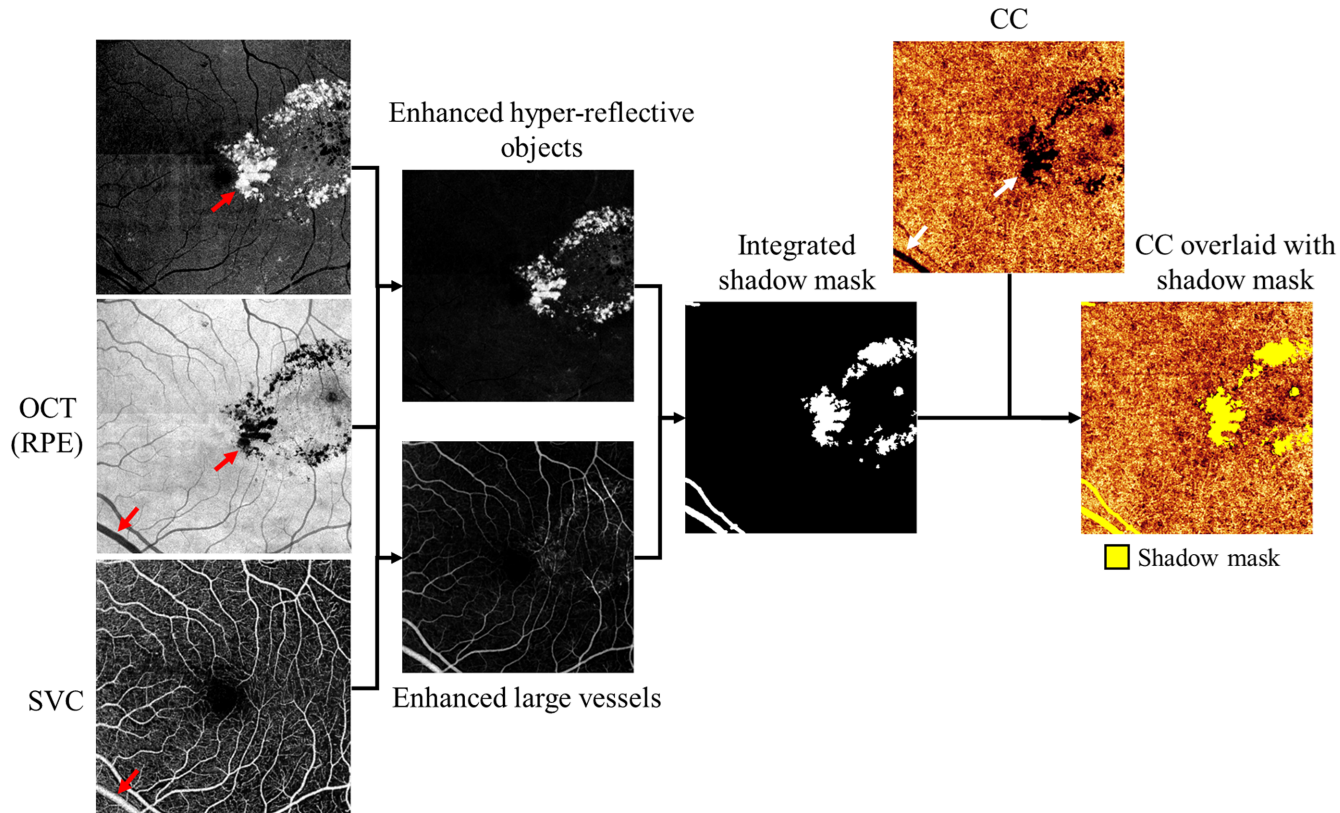


FIGURE 1. Shadow artifact detection. Hyperreflective objects were enhanced by multiplying the en face OCT within the DCP slab and the reflectance-reversed en face OCT of the RPE. Additionally, large vessels were enhanced by multiplying the SVC with the reflectance-reversed en face OCT of RPE. The hyperreflective object and large vessel mask were generated by setting separate thresholds on the enhanced images to exclude the shadow artifacts (highlighted in yellow) from the CC.

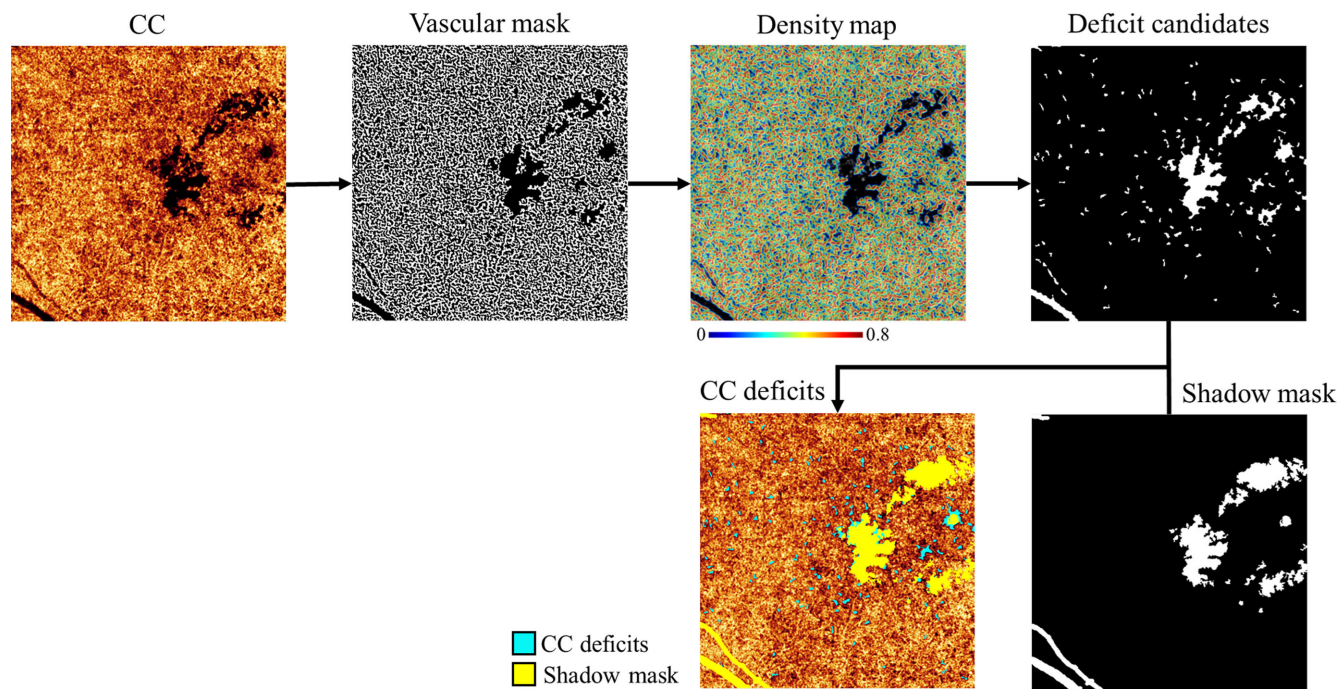


FIGURE 2. The proposed method for detecting CC deficits involves (1) generating an en face image using projection-resolved OCTA, (2) creating a vascular mask with a vascular enhancement algorithm, (3) producing a density map through low-pass filtering, (4) identifying deficit candidates via thresholding, (5) detecting shadowing from large vessels and hard exudates with structural OCT, and finally (6) confirming CC deficits by excluding shadowing areas.

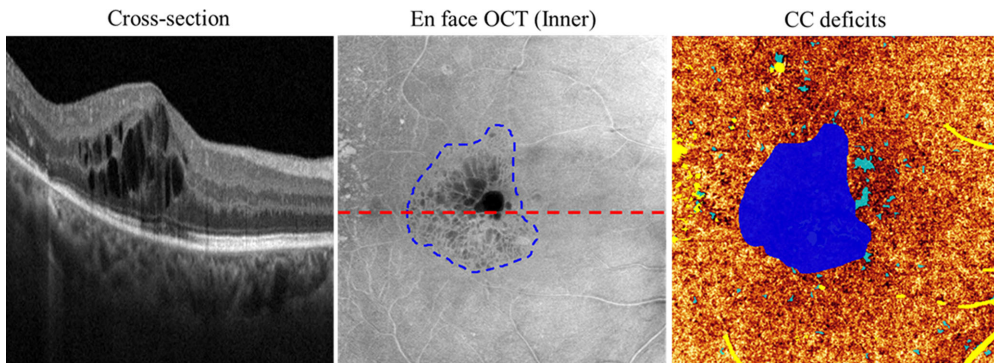


FIGURE 3. The retinal fluid area was manually annotated on the en face inner retina OCT image (second image) and verified on the cross-sectional OCT (first image). The CC deficit ratio was then measured after excluding both the area beneath the retinal fluid (blue) and shadows (yellow) (third image). The red dotted line on the en face OCT (inner) image denotes the location of the cross-sectional OCT.

reversed en face RPE image. The shadows caused by the floaters were detected by applying a threshold of 0.8 to the reversed en face RPE OCT image. These floaters also display hyperreflective areas in the enhanced image. Similarly, large vessels in the SVC slab were enhanced by multiplying the SVC with the reflectance-reversed en face RPE image. The large vessel mask was then generated from the enhanced large vessel image by using a threshold of 0.5. Masks for the hyperreflective objects and large vessels were then generated by setting thresholds on the enhanced images. Only larger, wider vessels can cause shadow artifacts in the CC image, so a threshold (0.06 mm) was also set on the detected vessel diameter to preserve only wider vessels in the mask.

Flow Deficit Detection

We identify flow deficits in the projection-resolved en face CC image (Fig. 2). To do so, we first enhance the vascular structure using the local contrast. Next, the image is binarized using Otsu's method.³⁵ From the binarized image, we then construct a flow density map using a low-pass filter with a $50 \times 50 \mu\text{m}$ size, applying axial length correction for each individual. Candidate flow deficits are identified by a density lower than 0.3. At this point, shadow-affected regions could still be included in the result. To prevent this, we use the shadow mask obtained from the shadow identification network to exclude such regions. Any remaining flow deficit candidates are then identified as CC deficits. The CC deficit ratio is measured by dividing the CC deficit area by the area of interest, excluding the shadowing area.

Effect of Retinal Fluid

Retinal fluid is a major pathology in eyes with DME and can cast shadows on the CC slab, raising concerns that it

may cause false-positive results and introduce bias into the analysis. To investigate the effect of retinal fluid and further mitigate the concerns of this potential bias in the analysis, the retinal fluid areas were manually sketched on the en face inner retina OCT image and verified on the cross-sectional images (Fig. 3). The CC deficit ratio was then measured by excluding both shadows and the area beneath the retinal fluid to assess the impact of retinal fluid on diagnosis performance.

RESULTS

Study Population

This is a retrospective cohort study; the dataset was collected as part of a DR study (R01 EY027833). We imaged one eye each from 183 participants with a range of DR severities (ANOVA, Tukey honestly significant difference (HSD), $P > 0.15$) (Table). The axial length of participants in the diabetes without DR group is significantly greater than all other groups (ANOVA, Tukey HSD, $P < 0.01$). The systolic blood pressure and diastolic blood pressure are matched across the groups (ANOVA, Tukey HSD, $P > 0.35$). The intraocular pressure in the NPDR group is significantly greater than normal controls (ANOVA, Tukey HSD, $P < 0.01$), but no significant differences were found among the other groups (ANOVA, Tukey HSD, $P > 0.15$). The signal strength index of the acquired OCTA scans is 72.65 ± 9.71 (mean \pm SD), with no significant differences among the groups ($P > 0.1$).

Qualitative Assessment

We visually inspected the validity of the CC deficit detected by our method (Fig. 4). Comparing with reflectance images

TABLE. Clinical Characteristics of Participants in Each Group of a Clinical DR Study

DR Severity	Normal Controls	Diabetes Without DR	NPDR	PDR
No. of eyes	76	7	64	36
Gender (Males/Females)	1.04	2.45	0.89	1.5
Age, mean \pm SD	49.75 ± 14.73	58.00 ± 14.14	53.94 ± 9.16	51.08 ± 11.55
Axial/Length (mm), mean \pm SD	23.82 ± 1.00	25.67 ± 1.55	23.67 ± 0.98	23.49 ± 1.13
Intraocular pressure (mm Hg), mean \pm SD	13.38 ± 2.35	14.86 ± 3.34	15.55 ± 2.98	14.72 ± 3.23
Systolic blood pressure (mm Hg), mean \pm SD	120.91 ± 17.85	121.33 ± 19.92	126.48 ± 19.55	127.97 ± 21.33
Diastolic blood pressure (mm Hg), mean \pm SD	75.47 ± 12.00	73.33 ± 11.55	74.53 ± 9.63	75.00 ± 11.80

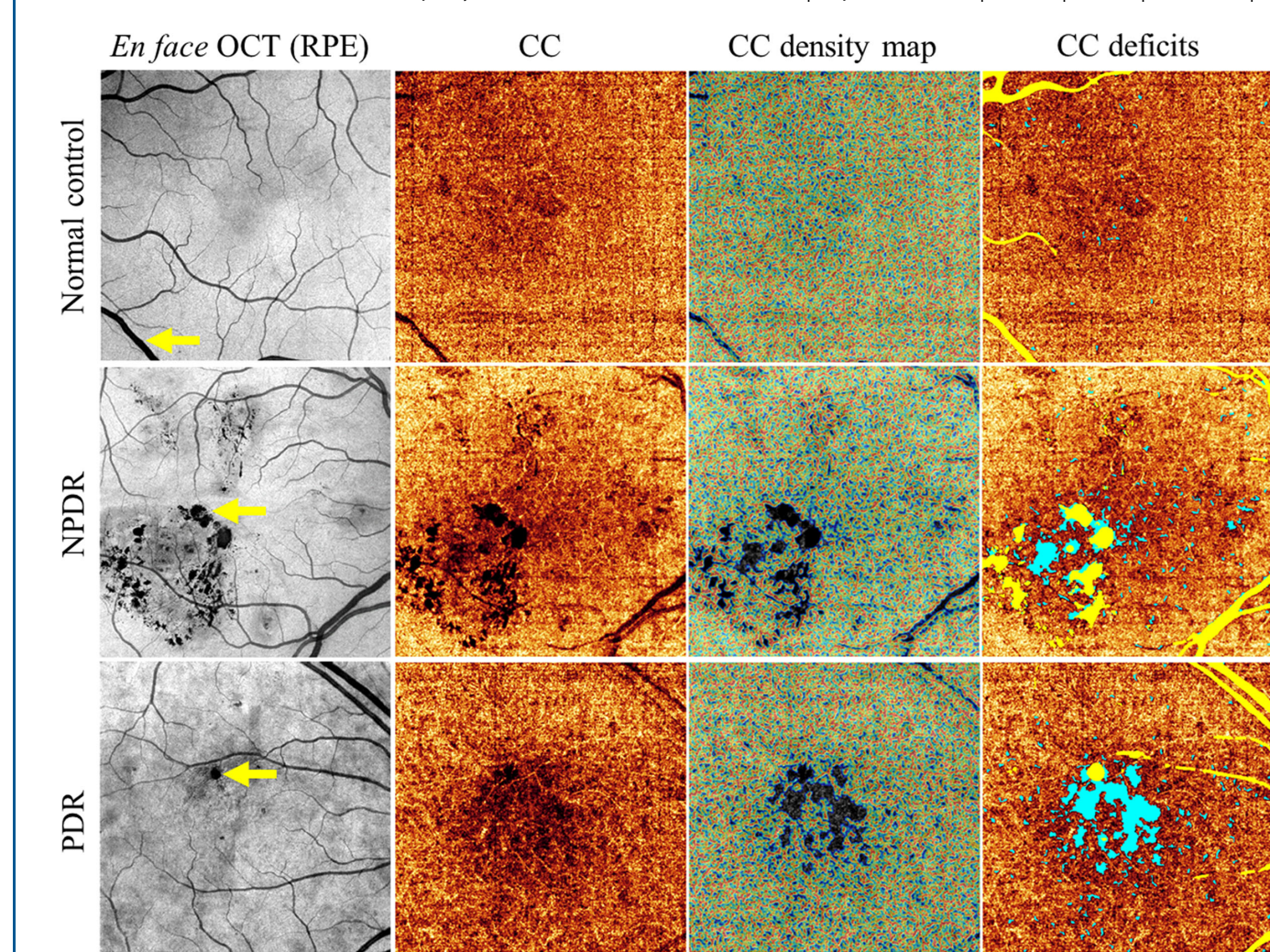


FIGURE 4. CC deficit detection for different DR severities. Shadow artifacts (highlighted by *yellow arrows*) caused by large vessels (row 1), hard exudates (row 2), and microaneurysms (row 3) had been excluded in the CC deficits (*light blue mask*) evaluation.

of the RPE, which is immediately anterior to the CC and on which shadows are readily identified, we found that our approach correctly identified shadows from hyperreflective material, hard exudates, and large vessels. As expected, the total number and size of deficits also increased with DR severity.

Quantitative Assessment

We then quantitatively assessed whether detected CC flow deficit metrics are meaningfully correlated to clinical disease. The CC deficit ratio measures the percentage of detected CC deficit area relative to the region of interest, excluding areas affected by shadow artifacts. By normalizing the deficit area over the imaging area, this metric is less sensitive to variations in axial length compared to raw area measurements.

First, we found a significant positive correlation between age and CC deficit ratio (Fig. 5) in normal controls (Pearson correlation, correlation coefficient = 0.43, $P = 0.02$). This is consistent with previous results from other groups³⁶ and represents a correlation that could be controlled for in diagnostic settings, similar to OCTA measurements of retinal vessel density.³⁷

Second, we compared the CC deficit ratio measurements between the exclusion of only shadows and those with the exclusion of both shadows and the area beneath the retinal fluid (Fig. 6). Forty-four normal controls under 50 years old were excluded to match the age criteria. The Mann-Whitney U-test showed no significant difference ($P = 0.81$), suggesting that the retina fluid did not affect the measurement using the proposed method.

And then, we examined the correlation between the CC deficit ratio and DR severity. We found that the CC deficit ratio is positively correlated with DR severity, with a Spearman correlation coefficient of 0.51 and 0.48 ($P < 0.01$ for both) for age-matched datasets with only shadows excluded and both the shadows and the area beneath retinal fluid excluded (Fig. 6). This suggests that CC deficit measurements, regardless of the effect of retinal fluid, are positively and moderately correlated with DR severity. We also found that the CC deficit ratio is correlated with visual acuity (LogMAR), with a Pearson correlation coefficient of 0.65 and 0.56 ($P < 0.01$ for both) for age-matched datasets with only shadows excluded and both shadows and the area beneath the retinal fluid excluded. With or without the area beneath the retinal fluid, the statis-

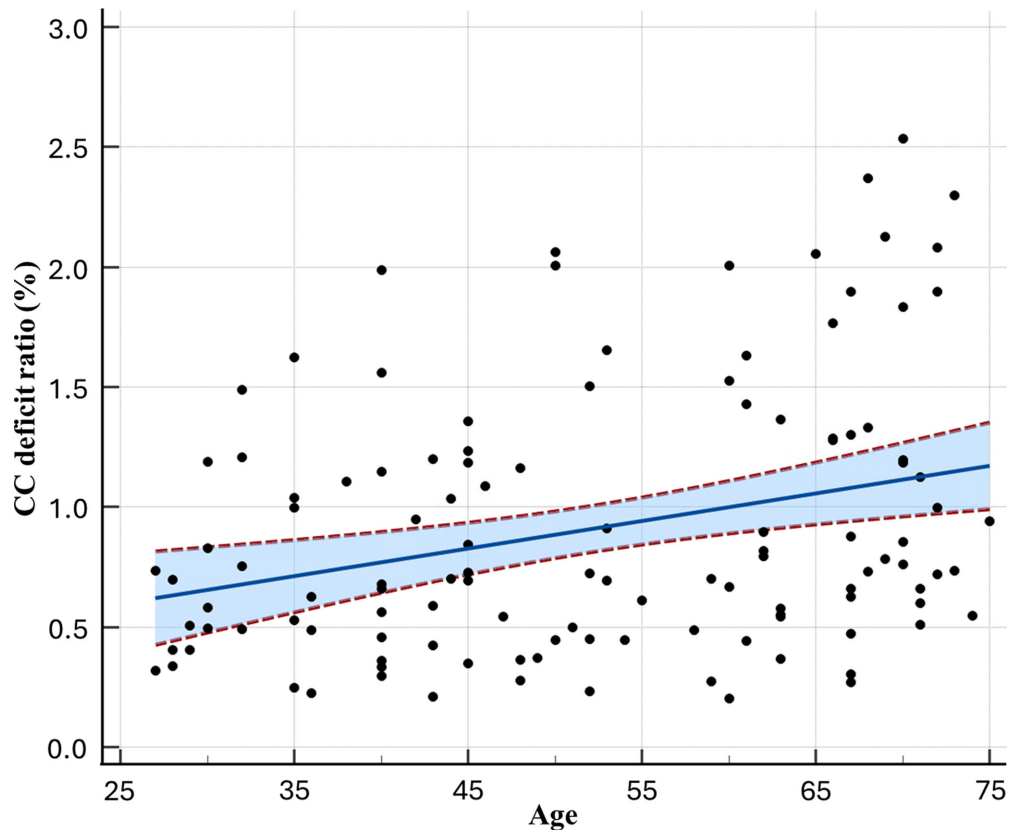


FIGURE 5. Scatter plot with linear regression showing age versus CC deficit ratio. The light blue–shaded region represents the 95% confidence interval.

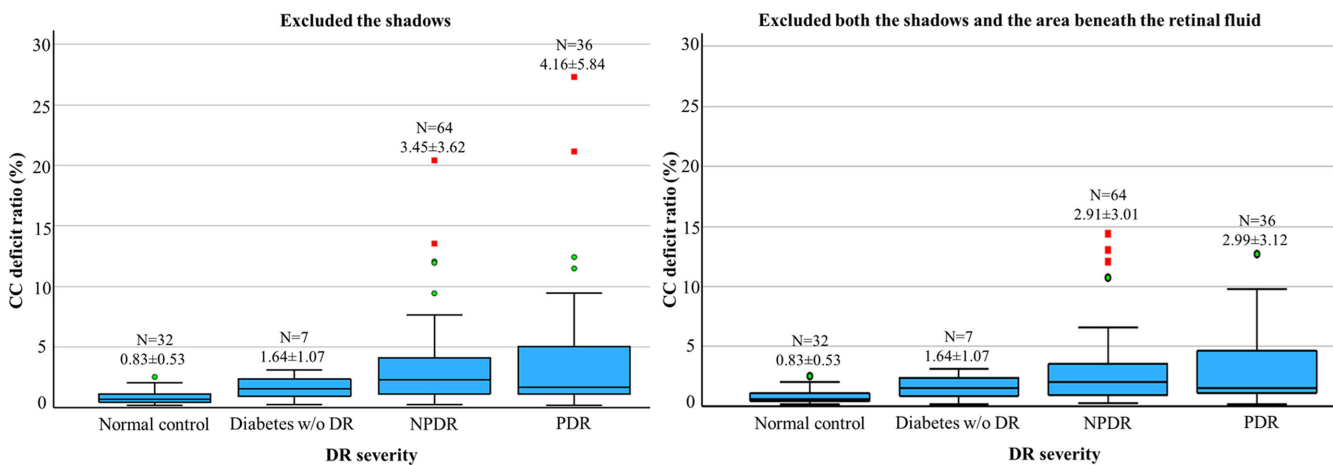


FIGURE 6. Box-and-whisker plot showing CC deficit ratio in relation to DR severity (Left: excluded the shadows; Right: excluded both the shadows and the area beneath the retinal fluid). The number of participants (N) and mean \pm standard deviation of CC deficit ratio are displayed at the top of each group.

tical analysis shows that the deficit ratio is significantly increased in NPDR and PDR compared to normal controls ($P < 0.01$), with no significant difference in diabetes without DR (ANOVA, Tukey HSD, $P > 0.8$). The CC deficit measurements (with area beneath the retinal fluid) had high repeatability, with an intraclass correlation coefficient of 0.92 ($n = 183$).

We evaluated whether the CC deficit ratio can determine clinically meaningful stages in DR (Fig. 7): (1) healthy controls versus eyes with diabetes, detecting pre-clinical retinal changes associated with diabetes; (2) eyes without DR (with or without diabetes mellitus) versus eyes with DR of any severity; (3) non-referrable eyes (including healthy controls, diabetes without DR, and

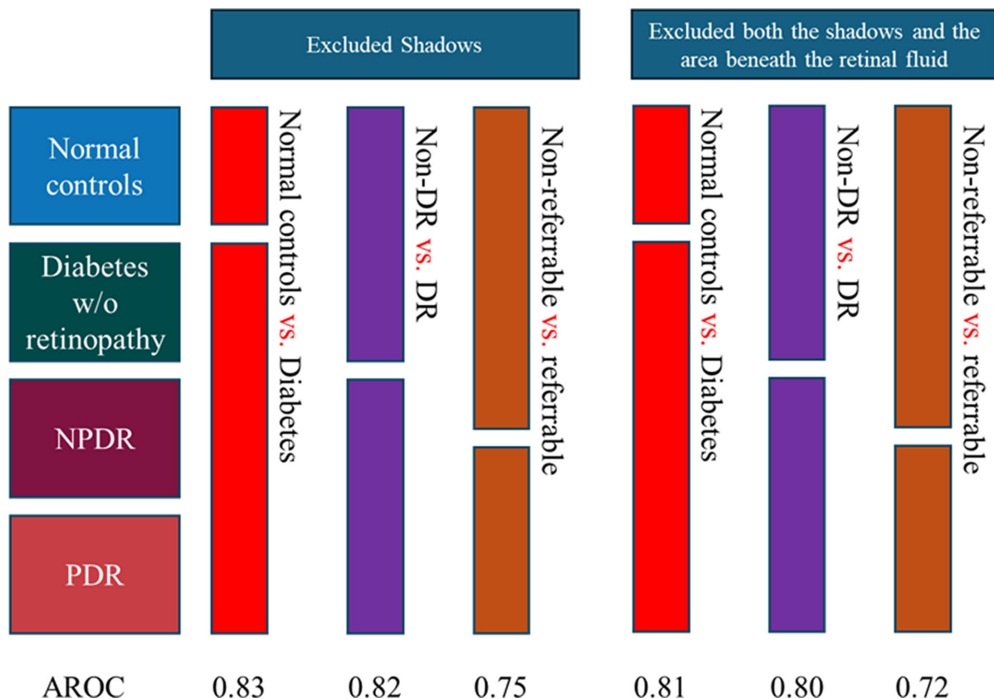


FIGURE 7. Area under the receiver-operating characteristic curve of CC deficit ratio for normal control eyes versus eyes with diabetes, eyes without DR (including both normal controls and eyes with diabetes mellitus) versus eyes with DR, non-referrable eyes versus referable eyes.

non-referrable DR) versus referable eyes (with referable DR).

DISCUSSION

In this work, we developed a CC deficit segmentation approach that provided CC deficit ratio (percent area) measurements correlating with volunteer age and DR severity. This approach was capable of diagnosing DR and identifying pre-clinical changes in the CC because of diabetes mellitus. We ensured the accuracy of our method by incorporating two key types of artifact compensation. First, we addressed projection artifacts using our volumetric signal attenuation compensation method, thereby minimizing false flow signal detection in the CC slab.³³ Second, we excluded regions with identified shadows, avoiding artificially low flow signals resulting in false-positive CC deficit detection. Together, these approaches avoid two important sources of mis-quantification in deficit segmentation.

Our method distinguishes itself from other CC deficit detection approaches by being specifically optimized for use in DR eyes. Many existing methods focus on age-related macular degeneration (AMD),³⁶ which presents different challenges compared to DR. For instance, drusen—a major feature of AMD—causes mild signal attenuation in the CC slab, but it is often possible to recover *in situ* flow information beneath them.^{26,38,39} In contrast, the method here excludes regions with signal attenuation, as features of DR, such as hard exudates or vitreous hemorrhage, make it impossible to recover flow information in the affected area, requiring exclusion from analysis.

We found that the CC deficit ratio can distinguish healthy eyes from diabetic eyes and DR eyes from eyes without DR.

This suggests that CC deficits could be a useful biomarker for the early detection of vasculopathy secondary to diabetes. Our results agree with previous studies that a higher deficit ratio is larger in eyes with DR than in healthy eyes.^{36,40} In other studies, deficits were shown to predict worsening severity.^{41,42}

Processing the area beneath retinal fluid is challenging, as fluid casts shadows and may lead to over-detection of CC deficits and introduce bias in the analysis. Conversely, CC deficits may indeed exist beneath the area of retinal fluid or even correlated with its occurrence; thus, excluding these areas may risk removing meaningful pathological information and compromise diagnostic performance. Specifically, the choriocapillaris endothelium is an important source of VEGF, there is a pathophysiologic rationale for a causal relationship between CC flow deficit and macular edema. It is important to note that the Mann-Whitney U-test showed no significant difference ($P = 0.81$) between the CC deficit ratio measurements with only shadows excluded and with both shadows and the area beneath the retinal fluid area excluded, suggesting that our proposed method is reliable in cases with signal attenuation due to the effect of retinal fluid. Studies have reported a decrease in choroidal thickness and vascularity following anti-VEGF therapy, primarily as a response to edema.^{43,44} However, CC is a thin lamellar vascular layer, and changes in choroidal thickness do not necessarily indicate a loss of CC perfusion. Nonetheless, this is worth investigating by examining CC deficits before and after anti-VEGF treatment, which could offer valuable insights into its effects on CC. Future work can specifically look at the relationship between CC flow deficit and DME.

Although diabetic choridopathy is a known entity, *in vivo* correlation between diabetic choridopathy and retinopa-

thy is not yet well established because of imaging-related challenges. The choriocapillaris endothelium is an important source of vascular endothelial growth factor and may have a role in the pathogenesis of neovascularization and macular edema.¹⁶ Furthermore, the site of energy absorption in photocoagulation, both for panretinal photocoagulation for proliferative diabetic retinopathy and macular focal grid photocoagulation for macular edema, occurs at the level of retinal pigment epithelium adjacent to the choriocapillaris. To date, directed treatment has focused on retinal vasculature, whether it is panretinal photocoagulation⁴⁵ or grid photocoagulation in the area of retinal nonperfusion. The ability to measure choriocapillaris disease in diabetic retinopathy may improve our understanding, not only of the disease process, but also response to treatment. Flow deficit quantifications are therefore an attractive candidate for inclusion in DR feature-based analysis alongside retinal pathologies (non-perfusion area, retinal neovascularization, etc.).

A limitation of this study is that it was conducted on a relatively small dataset, particularly for diabetes without DR group. A larger and more balanced dataset—including well-represented cases of diabetes without DR, NPDR, and PDR—would offer a more comprehensive understanding of the relationship between DR severity CC deficit ratio. The 3×3 mm scan pattern offers higher resolution but is more prone to shadowing effects. Therefore we selected a larger field of view (6.4×6.4 mm), which still provides sufficient resolution for visualizing and quantifying CC deficits. The absolute CC deficit area can be affected by the refractive differences, potentially introducing interindividual bias. To mitigate this, we measured the CC deficit ratio, defined as the proportion of the deficit area to the total analytical area, which can eliminate variation in the imaging resolution at the pixel level. However, the actual imaging region may vary slightly because of the refractive differences, introducing a potential limitation of this study. In this study, we found that CC deficit ratio is positively and moderately correlated with DR severity. Combining more biomarkers, such as vessel density, non-perfusion area, and thickness of the anatomic superficial, intermediate, and deep slabs, could increase the predictive value. A previous study suggested that ultra-wide field fluorescein angiography could improve the reliability of detecting unsuspected vision-threatening DR in eyes with clinically referable DR.⁴⁶ However, ultra-wide field fluorescein angiography is not always available for each enrolled patient, as it is an invasive imaging modality, and clinicians only order this imaging when deemed clinically necessary. And one grader in this study might introduce the potential subjective bias. These limitations highlight opportunities for future studies in CC by enhancing the grading procedures. Our data was also collected using a spectral-domain OCT, and the excluded shadow area could be smaller if we had worked with swept-source OCT instead. However, in both spectral domain and swept source systems, hard exudates, vitreous floaters, and large vessels can attenuate the flow signal, and we were careful to exclude these confounding factors. A potential concern may arise from the exclusion of the shadowing area, which can vary in individuals, and could introduce variability in the effective analytical area. While this limitation is not specific to our proposed methods, it is a common challenge regardless of the methodologies or imaging devices used. Another issue is that the validity of our approach is difficult to establish. Although a human-graded approach

could provide further validation, it is time-consuming and may involve subjective judgments about whether the CC flow void areas are due to real pathology or artifacts, potentially making it less interpretable than our rule-based method. However, our method is able to distinguish different DR severities, which may give a better indication that our measurements can assess physiologically relevant features in the CC, which is arguably more important than if they match human visual assessment. Additionally, the evolution of CC deficits in follow-up scans could provide valuable insights into the contributions of CC pathological changes as DR progresses.

In conclusion, the proposed method provided a reliable measurement of CC deficits with PR-OCTA and distinguished clinically meaningful levels of diabetic eye disease. This could improve our understanding of the role of choriocapillaris in the development of vision-threatening complications of DR, including DME and NV.

Acknowledgments

Supported by grants from National Institutes of Health (R01 EY 036429, R01 EY035410, R01 EY024544, R01 EY027833, R01 EY031394, R43EY036781, P30 EY010572, T32 EY023211, UL1TR002369); the Jennie P. Weeks Endowed Fund; the Malcolm M. Marquis, MD Endowed Fund for Innovation; Unrestricted Departmental Funding Grant and Dr. H. James and Carole Free Catalyst Award from Research to Prevent Blindness (New York, NY); Edward N. & Della L. Thome Memorial Foundation Award, and the Bright Focus Foundation (G2020168, M20230081).

Disclosure: **J. Wang**, Visionix/Optovue (P, R), Roche/Genentech (P, R), Ifocus Imaging (I, P); **T. Hormel**, Ifocus Imaging (I); **D.-W. Park**, None; **S. Haq**, None; **S. Bailey**, Visionix/Optovue, Inc. (F); **D. Huang**, Visionix/Optovue (F, P, R), Boehringer Ingelheim (C), Roche/Genentech (P, R), Cylite (F), Intalight (F), Kugler (R), Elsevier (R), GoCheck Kids (I, P), Stroma (I), Unfold Therapeutics (I, P), Visionix/Optovue, Inc. (F, P, R), Boehringer Ingelheim Inc. (C); **T.S. Hwang**, None; **Y. Jia**, Visionix/Optovue (P, R), Roche/Genentech (P, R, F), Ifocus Imaging (I, P), Optos (P), Boehringer Ingelheim (C), Kugler (R)

References

1. Leasher JL, Bourne RR, Flaxman SR, et al. Global estimates on the number of people blind or visually impaired by diabetic retinopathy: a meta-analysis from 1990 to 2010. *Diabetes Care*. 2016;39:1643–1649.
2. Wong TY, Sun J, Kawasaki R, et al. Guidelines on diabetic eye care: the international council of ophthalmology recommendations for screening, follow-up, referral, and treatment based on resource settings. *Ophthalmology*. 2018;125:1608–1622.
3. Teo ZL, Tham Y-C, Yu M, et al. Global prevalence of diabetic retinopathy and projection of burden through 2045: systematic review and meta-analysis. *Ophthalmology*. 2021;128:1580–1591.
4. Swanson E, Huang D. Ophthalmic OCT reaches \$1 billion per year. *Retin Physician*. 2011;8(4):58–59.
5. Flaxel CJ, Adelman RA, Bailey ST, et al. Diabetic retinopathy preferred practice pattern. *Ophthalmology*. 2020;127(1):P66–P145.
6. You QS, Guo Y, Wang J, et al. Detection of clinically unsuspected retinal neovascularization with wide-field optical coherence tomography angiography. *Retina*. 2020;40:891–897.

7. Tsuboi K, Mazloumi M, Guo Y, et al. Utility of en face OCT for the detection of clinically unsuspected retinal neovascularization in patients with diabetic retinopathy. *Ophthalmol Retina*. 2023;7:683–691.
8. Hwang TS, Gao SS, Liu L, et al. Automated quantification of capillary nonperfusion using optical coherence tomography angiography in diabetic retinopathy. *JAMA Ophthalmol*. 2016;134:367–373.
9. Decker NL, Duffy BV, Boughanem GO, et al. Macular perfusion deficits on OCT angiography correlate with nonperfusion on ultrawide-field fluorescein angiography in diabetic retinopathy. *Ophthalmol Retina*. 2023;7:692–702.
10. Schaal KB, Munk MR, Wyssmueller I, Berger LE, Zinkernagel MS, Wolf S. Vascular abnormalities in diabetic retinopathy assessed with swept-source optical coherence tomography angiography widefield imaging. *Retina*. 2019;39:79–87.
11. Kaizu Y, Nakao S, Wada I, et al. Microaneurysm imaging using multiple en face OCT angiography image averaging: morphology and visualization. *Ophthalmol Retina*. 2020;4:175–186.
12. Querques G, Borrelli E, Battista M, Sacconi R, Bandello F. Optical coherence tomography angiography in diabetes: focus on microaneurysms. *Eye*. 2021;35:142–148.
13. Gao M, Hormel TT, Guo Y, et al. Perfused and nonperfused microaneurysms identified and characterized by structural and angiographic OCT. *Ophthalmol Retina*. 2024;8:108–115.
14. Sun Z, Yang D, Tang Z, Ng DS, Cheung CY. Optical coherence tomography angiography in diabetic retinopathy: an updated review. *Eye*. 2021;35:149–161.
15. Campos A, Campos EJ, Martins J, Ambrósio AF, Silva R. Viewing the choroid: where we stand, challenges and contradictions in diabetic retinopathy and diabetic macular oedema. *Acta Ophthalmol*. 2017;95:446–459.
16. Lutty GA, McLeod DS, Merges C, Diggs A, Plouét J. Localization of vascular endothelial growth factor in human retina and choroid. *Arch Ophthalmol*. 1996;114:971–977.
17. Lutty GA. Effects of diabetes on the eye. *Invest Ophthalmol Vis Sci*. 2013;54(14):ORSF81–ORSF87.
18. Regatieri CV, Branchini L, Carmody J, Fujimoto JG, Duker JS. Choroidal thickness in patients with diabetic retinopathy analyzed by spectral-domain optical coherence tomography. *Retina*. 2012;32:563–568.
19. Adhi M, Brewer E, Waheed NK, Duker JS. Analysis of morphological features and vascular layers of choroid in diabetic retinopathy using spectral-domain optical coherence tomography. *JAMA Ophthalmol*. 2013;131:1267–1274.
20. Papasavvas I, Tucker WR, Mantovani A, Fabozzi I, Herbort CP. Choroidal vasculitis as a biomarker of inflammation of the choroid. Indocyanine Green Angiography (ICGA) spearheading for diagnosis and follow-up, an imaging tutorial. *J Ophthalmic Inflamm Infect*. 2024;14:1–36.
21. Ryu G, Moon C, van Hemert J, Sagong M. Quantitative analysis of choroidal vasculature in polypoidal choroidal vasculopathy using ultra-widefield indocyanine green angiography. *Sci Rep*. 2020;10(1):18272.
22. Singh RB, Perepelkina T, Testi I, et al. *Imaging-based assessment of choriocapillaris: A comprehensive review*. Abingdon, UK: Taylor & Francis; 2023:405–426.
23. Alm A, Bill A. Ocular and optic nerve blood flow at normal and increased intraocular pressures in monkeys (*Macaca irus*): a study with radioactively labelled microspheres including flow determinations in brain and some other tissues. *Exp Eye Res*. 1973;15:15–29.
24. Chu Z, Gregori G, Rosenfeld PJ, Wang RK. Quantification of choriocapillaris with optical coherence tomography angiography: a comparison study. *Am J Ophthalmol*. 2019;208:111–123.
25. Zhang Q, Shi Y, Zhou H, et al. Accurate estimation of choriocapillaris flow deficits beyond normal intercapillary spacing with swept source OCT angiography. *Quant Imaging Med Surg*. 2018;8:658.
26. Nesper PL, Fawzi AA. New method for reducing artifactual flow deficits caused by compensation techniques in the choriocapillaris with optical coherence tomography angiography. *Retina*. 2022;42:328–335.
27. Hormel TT, Huang D, Jia Y. Artifacts and artifact removal in optical coherence tomographic angiography. *Quant Imaging Med Surg*. 2021;11:1120.
28. Guo Y, Hormel TT, Xiong H, et al. Development and validation of a deep learning algorithm for distinguishing the nonperfusion area from signal reduction artifacts on OCT angiography. *Biomed Opt Express*. 2019;10:3257–3268.
29. Jia Y, Tan O, Tokayer J, et al. Split-spectrum amplitude-decorrelation angiography with optical coherence tomography. *Opt Express*. 2012;20:4710–4725.
30. Kraus MF, Potsaid B, Mayer MA, et al. Motion correction in optical coherence tomography volumes on a per A-scan basis using orthogonal scan patterns. *Biomed Opt Express*. 2012;3:1182–1199.
31. Zhang M, Wang J, Pechauer AD, et al. Advanced image processing for optical coherence tomographic angiography of macular diseases. *Biomed Opt Express*. 2015;6:4661–4675.
32. Hormel TT, Wang J, Bailey ST, Hwang TS, Huang D, Jia Y. Maximum value projection produces better en face OCT angiograms than mean value projection. *Biomed Opt Express*. 2018;9:6412–6424.
33. Wang J, Hormel TT, Bailey ST, Hwang TS, Huang D, Jia Y. Signal attenuation-compensated projection-resolved OCT angiography. *Biomed Opt Express*. 2023;14:2040–2054.
34. Jerman T, Pernuš F, Likar B, Špiclin Ž. Enhancement of vascular structures in 3D and 2D angiographic images. *IEEE Trans Med Imaging*. 2016;35:2107–2118.
35. Otsu N. A threshold selection method from gray-level histograms. *Automatica*. 1975;11(285–296):23–27.
36. Gendelman I, Alibhai AY, Moult EM, et al. Topographic analysis of macular choriocapillaris flow deficits in diabetic retinopathy using swept-source optical coherence tomography angiography. *Int J Retina Vitreous*. 2020;6:1–8.
37. Gao SS, Jia Y, Liu L, et al. Compensation for reflectance variation in vessel density quantification by optical coherence tomography angiography. *Invest Ophthalmol Vis Sci*. 2016;57:4485–4492.
38. Zhang Q, Zheng F, Motulsky EH, et al. A novel strategy for quantifying choriocapillaris flow voids using swept-source OCT angiography. *Invest Ophthalmol Vis Sci*. 2018;59:203–211.
39. Ledesma-Gil G, Fernandez-Avellaneda P, Spaide RF. Swept-source optical coherence tomography angiography image compensation of the choriocapillaris induces artifacts. *Retina*. 2020;40:1865–1872.
40. Dai Y, Zhou H, Zhang Q, et al. Quantitative assessment of choriocapillaris flow deficits in diabetic retinopathy: a swept-source optical coherence tomography angiography study. *PLoS one*. 2020;15(12):e0243830.
41. Chen Y, Zhu Z, Cheng W, et al. Choriocapillaris flow deficit as a biomarker for diabetic retinopathy and diabetic macular edema: 3-year longitudinal cohort. *Am J Ophthalmol*. 2023;248:76–86.
42. Wang W, Cheng W, Yang S, Chen Y, Zhu Z, Huang W. Choriocapillaris flow deficit and the risk of referable diabetic retinopathy: a longitudinal SS-OCTA study. *Br J Ophthalmol*. 2023;107:1319–1323.

43. Yiu G, Manjunath V, Chiu SJ, Farsiu S, Mahmoud TH. Effect of anti-vascular endothelial growth factor therapy on choroidal thickness in diabetic macular edema. *Am J Ophthalmol.* 2014;158:745–751. e2.
44. Minnella AM, Centini C, Gambini G, et al. Choroidal thickness changes after intravitreal aflibercept injections in treatment-naïve neovascular AMD. *Adv Ther.* 2022;39:3248–3261.
45. Wilson DJ, Green WR. Argon laser panretinal photocoagulation for diabetic retinopathy: scanning electron microscopy of human choroidal vascular casts. *Arch Ophthalmol.* 1987;105:239–242.
46. Castellanos-Canales D, Decker NL, Fukuyama H, Duffy BV, Fawzi AA. Reliability of clinical grading of diabetic retinopathy compared with grading of ultra-widefield images. *Retina.* 2024;44:1279–1287.